Available online at www.sciencedirect.com
ScienceDirect
Ceramics International 35 (2009) 3073–3079
CERAMICS INTERNATIONAL
www.elsevier.com/locate/ceramint

# Sol–gel approach to near-net-shape oxide–oxide composites reinforced with short alumina fibres—The effect of crystallization

Milan Kanti Naskar [a,*], Kunal Basu [b], Minati Chatterjee [a]

[a] Sol-Gel Division, Central Glass and Ceramic Research Institute (CSIR), Kolkata 700032, India
[b] Sagar Institute of Science and Technology, Gandhi Nagar, Bhopal 462034, India

Received 24 July 2008; received in revised form 12 March 2009; accepted 14 April 2009
Available online 21 May 2009

**Abstract**

Near-net-shape (NNS) high alumina (alumina:silica = 96:4, in equivalent weight ratio) fibre reinforced ceramic matrix composites (CMCs) were prepared with single and bicomponent sols following sol–gel vacuum infiltration technique. The CMCs were characterized by X-ray diffraction (XRD), three-point bend test and scanning electron microscopy (SEM). Crystallization of tetragonal zirconia (t-$ZrO_2$) in the composite, CZY having zirconia–yttria matrix and that of gamma alumina ($\gamma$-$Al_2O_3$) in the composites, CAZ having alumina–zirconia matrix, CAS having alumina–silica matrix and CA having alumina matrix, enhanced the flexural strength values and pseudo-ductile character of CMCs.


*Keywords:* A. Sol–gel process; B. Fibres; B. Composites; C. Mechanical properties; E. Structural applications

## 1. Introduction

The use of monolithic ceramics has some restrictions in structural applications because of their inherent catastrophic nature. The development of ceramic fibre reinforced ceramic matrix composites (CMCs) has been proved to be promising alternative to monolithic ceramics for structural materials fabrication in engineering field [1,2]. If CMCs could be made consistently and at reasonable cost, they could be ideal for high temperature corrosive and abrasive environments. One of the processes of fabrication of CMCs is to infiltrate a liquid matrix into a reinforcement assemblage of required shape and size which is called preform [2]. These preforms may be continuous or discontinuous fibres or whiskers or particulates assemblages prepared to the desired volume fraction, shapes and sizes [2,3].

Several techniques are currently used to fabricate CMCs with NNS capability which is used to produce NNS components that do not require machining or working with diamond tools. The conventional methods of producing CMCs are hot pressing [4], melt infiltration [5], chemical vapour infiltration (CVI) [6], slurry infiltration-high pressure sintering (SI-HPS) [3,7,8] and sol–gel [3,8–14]. Radsick et al. [8] fabricated oxide/oxide matrix composites by slurry infiltration-hot pressing sintering technique (SI-HP). Recently Ruggles-Wrenn et al. [14] have studied the environmental effects on the creep behaviours of oxide/oxide ceramic matrix composites prepared by sol–gel technique. Dey et al. [11] have fabricated near-net-shape fibre reinforced ceramic matrix composites by sol infiltration technique. Sol–gel vacuum infiltration technique is a promising route for the fabrication of oxide–oxide ceramic matrix composite. In the vacuum infiltration technique, a solution containing metal compounds, e.g., metal alkoxides, acetates, nitrates or halides are treated chemically to form a sol which is then infiltrated into the fibre preform. The sol in the preform is converted to gel form by physical and/or chemical means, which in turn is subjected to control heating to produce the desired products e.g., glass, glass–ceramic or ceramic matrix. The main advantages of this technique are lower processing temperature and higher compositional homogeneity with respect to slurry infiltration-hot pressing sintering technique (SI-HP). In this process, preforms provide a uniform distribution of fibres and a very high surface area to the matrix gel. However, during drying, shrinkage of matrix results in crack formation in the matrix. It can be minimized by repeated infiltrations with the sol matrix and subsequent drying.

The properties of CMCs are influenced by the characteristics of the reinforcing fibres i.e., their strength, aspect ratio,

* Corresponding author. Tel.: +91 33 2483 8086; fax: +91 33 2473 0957.
*E-mail address:* milan@cgcri.res.in (M.K. Naskar).

0272-8842/$36.00 
doi:10.1016/j.ceramint.2009.04.013

chemistry and thermal stability [2,15]. The use of sintering aid also influenced the mechanical strength of the CMC [16]. For the development of a high quality CMC, matrix properties are also to be taken into account. Important characteristics of the matrix include thermal compatibility with the fibres and fibre–matrix interface reaction. The strength and toughness of CMC are primarily governed by the interfacial bonding at the fibre/matrix interface [1,15]. Interfacial strength can be influenced by a number of factors, most important being degree of bonding between the fibre and the matrix and their difference in thermal expansion behaviour.

Crystallization behaviour i.e., the development of crystalline phases in the composites with sintering temperatures has an important role for the characteristics of the CMCs. In the present investigation, a sol–gel vacuum infiltration route was followed for the preparation of NNS ceramic fibre reinforced ceramic matrix composites using various sols as the infiltrates. The effect of crystallization in the composites towards their characteristics i.e., mechanical strength, pseudo-ductility and hence the nature of fibre–matrix interface has been studied in this work.

## 2. Experimental procedure

### 2.1. Preparation of precursor sols

Zirconium oxychloride octahydrate, $ZrOCl_2{\cdot}8H_2O$ (Indian Rare Earths Ltd., Mumbai, India, purity > 99%), hydrated yttrium nitrate (Indian Rare Earths Ltd., Mumbai, India, purity > 99%), aluminum nitrate, $Al(NO_3)_3{\cdot}9H_2O$ (G.R. Merck, Mumbai, India, purity > 99%) and tetraethylorthosilicate, TEOS (Fluka Chemie AG, Switzerland, purity > 98%) were used as the starting materials for $ZrO_2$, $Y_2O_3$, $Al_2O_3$ and $SiO_2$ respectively. Fig. 1 shows schematically the preparative steps of zirconia–yttria (ZY), alumina–zirconia (AZ), alumina (A) and alumina–silica (AS) sols.

For the preparation of ZY sol with the composition $94ZrO_2{\cdot}6Y_2O_3$ (in equivalent mole), $ZrOCl_2{\cdot}8H_2O$ (1.5 M) was precipitated as hydrated zirconia by the addition of aqueous ammonia solution (25 wt.%, G.R. Merck, Mumbai, India) under stirring, maintaining the pH of the solution up to 8–9. The precipitate was washed with deionized water to free foreign ions e.g., $Cl^-$, $NH_4^+$ etc. followed by peptization with glacial acetic acid (99.8%, AnalaR, BDH, Mumbai, India) at 65 ± 1 °C. A required amount of $Y(NO_3)_3$ (6 mol% equivalent $Y_2O_3$) solution was added to the above peptized zirconia sol under stirring for 15 min at r.t (30 °C) to prepare ZY sol (Fig. 1).

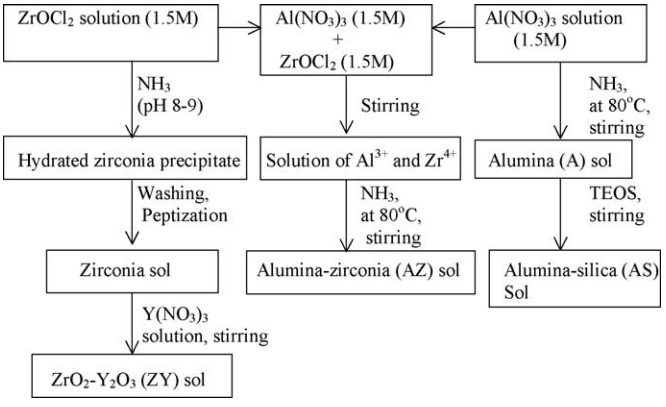


Fig. 1. Schematic for the preparation of zirconia–yttria (ZY), alumina–zirconia (AZ), alumina (A) and alumina–silica (AS) sols.

For the preparation of AZ sol of composition $87Al_2O_3{\cdot}13ZrO_2$ (in equivalent mole), required amount of $Al(NO_3)_3$ solution (1.5 M) was mixed with required amount of $ZrOCl_2$ solution (1.5 M) under stirring for 15 min. An aqueous ammonia solution (25 wt.%, G.R. Merck, Mumbai, India) was added to the above mixed solution containing $Al^{3+}$ and $Zr^{4+}$ under stirring at 80 ± 1 °C in a covered container (Fig. 1). In this case the adjustment of pH at around 3 is the crucial step for stabilizing of AZ sol.

For the preparation of alumina sol (A), ammonia solution (25 wt.% G.R. Merck, Mumbai, India) was slowly added to 1.5 M of $Al(NO_3)_3$ solution at 80 ± 1 °C under stirring in a covered container. The pH of the sol (A) was then adjusted up to about 3 by control addition of $NH_4OH$ in warm condition (Fig. 1).

A calculated quantity TEOS was slowly added under stirring to the required amount of alumina sol (A) as prepared above under stirring to obtain AS sol of composition $60Al_2O_3{\cdot}40SiO_2$ (in equivalent mole). The stirring was continued for 15 min for homogenization (Fig. 1).

The viscosity values of the above sols (ZY, AZ, A and AS) were adjusted up to either 10 or 5 mPa s by solvent evaporation. Two series of sols were prepared with different viscosities: one with a viscosity of 10 mPa s for the very first infiltration steps and the other with a viscosity of 5 mPa s for the last infiltration step(s).

### 2.2. Infiltration of the sols in the high alumina fibre preforms

In the present investigation, the high alumina fibre preform (M/s Thermal Ceramics, USA) (fibre content = 30 vol.%, length = 200–250 μm, diameter = 3–7 μm) of dimension 125 mm (diameter) × 25 mm (thickness) was infiltrated with the above prepared sols, ZY, AZ, AS and A using a custom-designed set-up (Fig. 2). In this technique, the fibre preform was placed on a filter bed (sintered disc) of the infiltration unit with the help of a specimen holder. The preform was immersed with the prepared sol of viscosity 10 mPa s by sucking it up through the filter bed with the help of a rotary vacuum pump attached to the infiltration unit. The samples were kept for 5 min in the sol under immersed condition followed by releasing pressure. The sol infiltrated preform was dried at 100 °C to convert the penetrated sol into the corresponding wet gel. This process was continued thrice with the same sol of viscosity 10 mPa s. The wet infiltrated preform was then heated at 400 °C in air under static condition to remove the volatiles and decomposable materials. Finally, the 400 °C-treated sample was infiltrated following the above procedure with the sol of viscosity 5 mPa s followed by heating at different temperatures, i.e., 800–1400 °C in air under static condition.

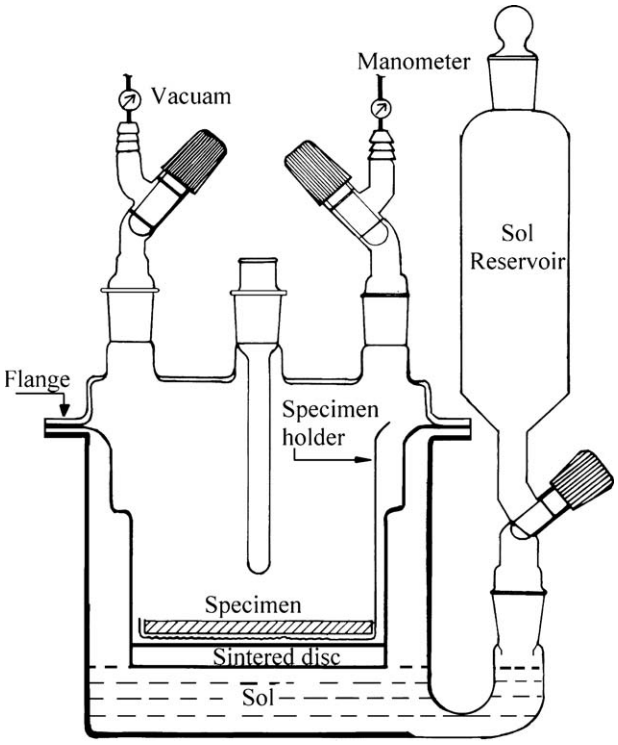


Fig. 2. Schematic of the sol infiltration set-up for the fabrication of near-net-shape ceramic fibre reinforced ceramic matrix composites.

### 2.3. Characterization of the materials

The infiltrates (sols) were characterized by measuring their pH with a Jencons pH meter (Model 3030, Jencons Scientific Ltd., Bedfordshire, U.K.) while the viscosity values were recorded using a Brookfield viscometer (Model LVTDV II, Brookfield Laboratories, Inc., MA, USA).

Crystallization behaviour of the matrix materials, fibre preform and the composites after firing at different temperatures i.e., 800–1400 °C was studied by X-ray diffraction (XRD) (Philips PW-1730 Philips Corporation, Almelo, the Netherlands) with Ni-filtered $CuK_\alpha$ radiation. The flexural strength of the composites was determined by Instron Universal Testing Machine, U.K. (Model: 5500 R). The samples of dimensions 40 mm × 7 mm × 6 mm were cut from the infiltrated preform for testing. For the measurement of flexural strength, three-point bend test under a crosshead speed of 0.5 mm/min was performed. The three-point bending stress, $\sigma$ is determined by the following equation [2]:

$$\sigma = \frac{3PL}{2bh^2}$$

where $P$ is the load at break, $L$ is the span length and $b$ and $h$ are the width and thickness of the test specimen respectively. Each strength datum is an average over six samples. Microstructural studies of the fibre preform and the composite materials were performed by scanning electron microscopy (SEM) (S 430i, LEO Electronic Microscopy Ltd., Cambridge, U.K.).

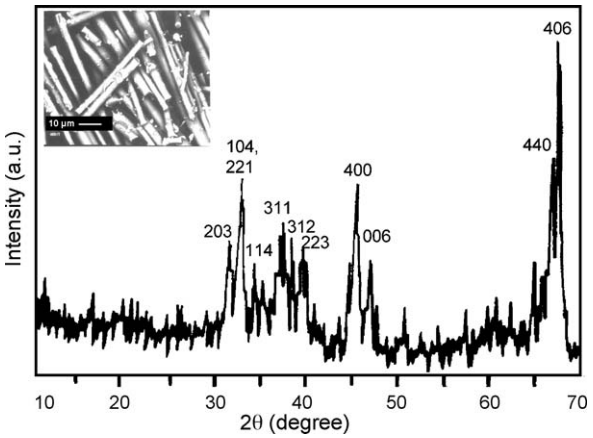


Fig. 3. XRD pattern and SEM image (inset) of high alumina fibre preform.

## 3. Results and discussion

The XRD of the precursor preforms used in the present investigation indicated the presence of δ-$Al_2O_3$ as the only crystallized phase (Fig. 3). The microstructure of the fibre preforms shows the presence of inter-fibre pores and voids (inset of Fig. 3). It indicates that the fibres are circular in diameter with range of 3–7 μm. The presence of considerable amount of inter-fibre pores and voids is evident from the microstructure. Infiltration of the sols in the preform is expected to fill these inter-fibre pores and voids, leading to the formation of the continuous phase, i.e., matrix.

In the present investigation, the fibre preforms were infiltrated with the sols of viscosity 10 ± 1 mPa s followed by intermediate heating at 400 °C. Finally, infiltrations were carried out with the sols of viscosity 5 ± 1 mPa s which helped to minimize matrix cracking and improve mechanical strength of CMCs [17]. It is to be noted that most of the interconnected pores and voids of the fibre preform were filled with the sol of higher viscosity followed by filling of residual pores and voids with the sol of lower viscosity.

Crystallization features of the matrix (in the absence of fibres) and fibre preform calcined at different temperatures i.e., 800–1400 °C are summarized in Tables 1a and 1b respectively. In case of MZY (M stands for matrix) matrix in zirconia–yttria system, a mixture of monoclinic (m-) and tetragonal (t-) zirconia ($ZrO_2$) was found at 800–1000 °C while they transformed to cubic (c-) and t-$ZrO_2$ at 1200–1400 °C. For MAZ (M stands for matrix) matrix in alumina–zirconia system, delta (δ-), gamma (γ-) $Al_2O_3$ and t-$ZrO_2$ were obtained at 800–1000 °C while α-$Al_2O_3$, t- and c-$ZrO_2$ were found at 1200–1400 °C. The appearance of γ-$Al_2O_3$ with amorphous silica was revealed for the sample MAS (M stands for matrix) matrix in alumina silica system at 800–1000 °C followed by their transformation to orthorhombic mullite phase at 1200–1400 °C. The sample MA (M stands for matrix) matrix in alumina system showed γ-$Al_2O_3$ at 800 °C, γ- and δ-$Al_2O_3$ at 1000 °C and α-$Al_2O_3$ at 1200–1400 °C.

The fibre preforms (FP) after sintering up to 1200 °C crystallized with δ- and θ-$Al_2O_3$ along with a trace amount of α-$Al_2O_3$ and orthorhombic mullite phase (Table 1b). A

Table 1a
XRD results of matrix (M) materials calcined 1 h at different temperatures.

| Sample designation | Calcination temperature (°C) | Crystalline phases |
|---|---|---|
| MZY | 800 | m- + t- |
| | 1000 | m- + t- |
| | 1200 | c- + t- |
| | 1400 | c- + t- |
| MAZ | 800 | δ- + γ- + t- |
| | 1000 | δ- + γ- + t- |
| | 1200 | α- + t- + c- |
| | 1400 | α- + t- + c- |
| MAS | 800 | γ- + $SiO_2$ (amorphous) |
| | 1000 | γ- + $SiO_2$ (amorphous) |
| | 1200 | mul |
| | 1400 | mul |
| MA | 800 | γ- |
| | 1000 | γ- + δ- |
| | 1200 | α- |
| | 1400 | α- |

*Note*: c-, cubic $ZrO_2$; t-, tetragonal $ZrO_2$; γ-, γ-$Al_2O_3$; α-, α-$Al_2O_3$; δ-, δ-$Al_2O_3$; mul, orthorhombic mullite.

Table 1b
XRD results of fibre preform (FP) calcined 1 h at different temperatures.

| Sample designation | Calcination temperature (°C) | Crystalline phases |
|---|---|---|
| FP8 | 800 | δ- + θ- + α- (trace) + mul (trace) |
| FP10 | 1000 | δ- + θ- + α- (trace) + mul (trace) |
| FP12 | 1200 | δ- + θ- + α- + mul (trace) |
| FP14 | 1400 | α- (major) + mul (minor) |

*Note*: θ-, θ-$Al_2O_3$.

substantial quantity of α-$Al_2O_3$ was found along with a small amount of mullite phase for 1400 °C-treated sample.

Crystallization behaviours of the CMCs (CZY, CAZ, CAS and CA, here C stands for composite) at different temperatures are depicted in Fig. 4. XRD of composite material CZY, with zirconia–yttria matrix, showed m- and t-$ZrO_2$ along with δ- and θ-$Al_2O_3$ up to 1200 °C. A mixture of t- and c-$ZrO_2$ along with a trace amount of α-$Al_2O_3$ and orthorhombic mullite phases each was obtained at 1400 °C.

All the composites (CAZ, CAS and CA) prepared with alumina–zirconia, alumina–silica and alumina matrices respectively, showed a significant amount of δ-, θ- and γ-$Al_2O_3$ at 800–1000 °C. The α-$Al_2O_3$ which appeared at 1200 °C became prominent at 1400 °C. At 1200 °C, along with the other polymorphs of alumina, t- and c-$ZrO_2$ were found in CAZ and orthorhombic mullite was obtained in CAS and CA. At 1400 °C, the α-$Al_2O_3$ and mullite were obtained in CAS and CA composites while CAZ crystallized with α-$Al_2O_3$, t-, c-$ZrO_2$ and trace amount of mullite.

The load displacement curves of the composites, CZY, CAZ, CAS and CA sintered at 800–1400 °C each are shown in Fig. 5. It is evident from the features of the curves that all the samples, heat treated at 800–1000 °C indicate some pseudo-ductile character showing steady falls of load elongation curves after

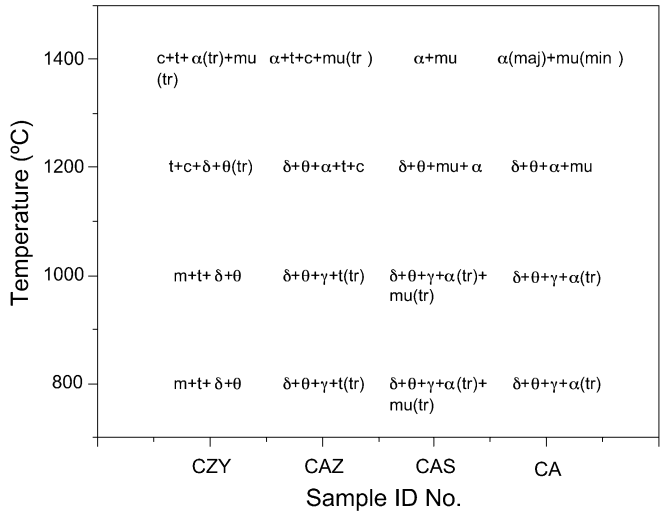


Fig. 4. Change in crystalline phases of the composites, CZY, CAZ, CAS and CA at different temperatures. m, monoclinic $ZrO_2$; t, tetragonal $ZrO_2$; c, cubic $ZrO_2$; γ, γ-$Al_2O_3$; α, α-$Al_2O_3$; δ, δ-$Al_2O_3$; θ, θ-$Al_2O_3$; mu, orthorhombic mullite.

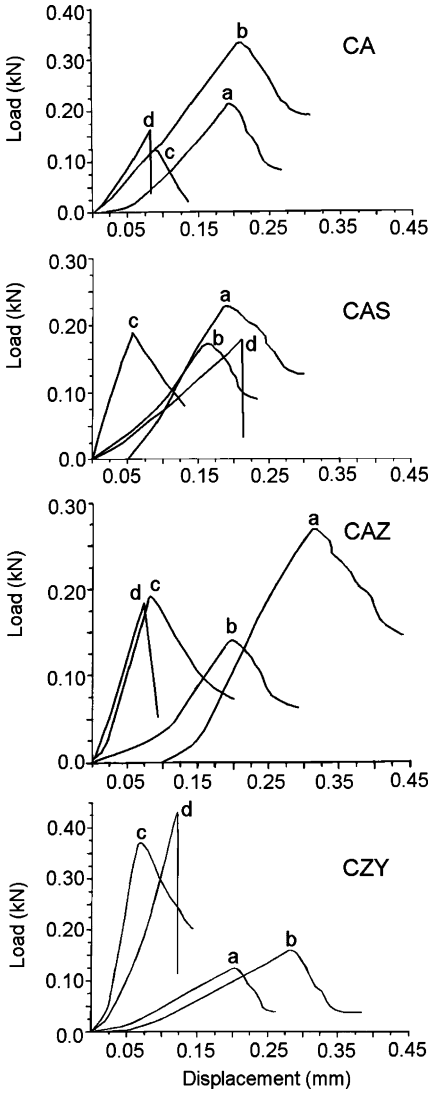


Fig. 5. Load displacement curves of the composites CZY, CAZ, CAS and CA each sintered at (a) 800 °C, (b) 1000 °C, (c) 1200 °C and (d) 1400 °C.

Table 2
Flexural strength of the composites calcined at different temperatures.

| Sample designation | Sol viscosity (mPa s) | Total no. of infiltration | Final sintering temperature (°C) | Flexural strength (MPa) |
|---|---|---|---|---|
| CZY | 10 ± 1 (3), 5 ± 1 (1) | 4 | 800 | 13.67 |
| | 10 ± 1 (3), 5 ± 1 (1) | 4 | 1000 | 15.86 |
| | 10 ± 1 (3), 5 ± 1 (1) | 4 | 1200 | 21.30 |
| | 10 ± 1 (3), 5 ± 1 (1) | 4 | 1400 | 31.08 |
| CAZ | 10 ± 1 (2), 5 ± 1 (2) | 4 | 800 | 18.48 |
| | 10 ± 1 (2), 5 ± 1 (2) | 4 | 1000 | 19.90 |
| | 10 ± 1 (2), 5 ± 1 (2) | 4 | 1200 | 14.34 |
| | 10 ± 1 (2), 5 ± 1 (2) | 4 | 1400 | 14.76 |
| CAS | 10 ± 1 (1), 5 ± 1 (3) | 4 | 800 | 21.71 |
| | 10 ± 1 (1), 5 ± 1 (3) | 4 | 1000 | 23.94 |
| | 10 ± 1 (1), 5 ± 1 (3) | 4 | 1200 | 19.54 |
| | 10 ± 1 (1), 5 ± 1 (3) | 4 | 1400 | 22.02 |
| CA | 10 ± 1 (1), 5 ± 1 (3) | 4 | 800 | 19.98 |
| | 10 ± 1 (1), 5 ± 1 (3) | 4 | 1000 | 21.23 |
| | 10 ± 1 (1), 5 ± 1 (3) | 4 | 1200 | 14.31 |
| | 10 ± 1 (1), 5 ± 1 (3) | 4 | 1400 | 16.27 |

*Note*: (i) intermediate sintering temperature = 400 °C/h; (ii) figures in parenthesis indicate the number of infiltration.

certain loads. Conversely, a brittle ceramic character is noticed for the samples sintered at 1200–1400 °C indicating sudden fall of load elongation curves after certain loads. Table 2 shows the flexural strength values of the composites sintered at 800–1400 °C along with the preceding infiltration steps of the sols into the fibre preforms. The change in flexural strength with sintering temperatures for the composites CZY, CAZ, CAS and CA is shown in Fig. 6.

The flexural strength of the composite, CZY increased continuously with the increase in sintering temperature from 800 to 1400 °C (Fig. 6). At relatively low sintering temperatures i.e., 800–1000 °C, the flexural strength values were quite low but increased sharply after 1000 °C. The SEM fractograph (Fig. 7a) of the sample CZY sintered at 1000 °C after three-point bending test showed pseudo-ductile character with fibre pull-out resulting from the development of weak fibre–matrix interface. Pseudo-ductility of the material was observed due to presence of $Y_2O_3$ as dopant in $ZrO_2$ host which helped to retain t-$ZrO_2$ (Fig. 4) inhibiting grain growth in the fibre–matrix interface. The material sintered at 1200–1400 °C showed ceramic character resulting in higher flexural strength values (Fig. 6). The strong interaction at the fibre–matrix interface developed at 1400 °C (Fig. 7b), the material becoming ceramic in nature. With increasing sintering temperatures, the materials became highly dense with the formation of strong fibre–matrix interface which resulted in higher flexural strength with some sorts of ceramic brittleness.

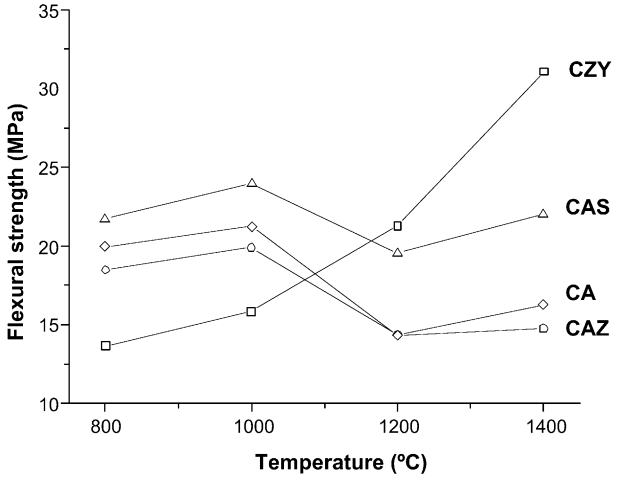


Fig. 6. Change in flexural strength of the composites, CZY, CAZ, CAS and CA with different temperatures: (□) CZY, (○) = CAZ, (△) = CAS and (◇) = CA.

It is interesting to point out that the flexural strength of the composites with an alumina-containing matrix (CAZ, CAS and CA) increased slightly with increase in temperature from 800 to 1000 °C (Fig. 6). However, it decreased significantly at 1200 °C followed by slight increase with increase in temperature from 1200 to 1400 °C. The decrease in flexural strength values at 1200 °C is due to the phase transformation of transient γ-$Al_2O_3$ to the stable α-$Al_2O_3$ (Fig. 4) accompanying the grain growth of the matrix [18,19] and fibres at the fibre–matrix interface. The better densification of the materials at 1400 °C resulted in slight increase of flexural strength values. Fig. 8a and b shows the SEM fractographs of the composites, CAZ and CA respectively sintered at 1000 °C each after three-point bend test. The fibre pull-out with relatively weak interaction at fibre–matrix interface is revealed from the microstructures. It indicated pseudo-ductility of the composites. Fig. 9a and b shows the fracture surfaces of the composites, CAS and CA respectively sintered at 1400 °C each. It revealed the formation of strong bonding between fibres and matrix of the composites indicating brittle ceramic character.

It is to be noted that for all the composites CZY, CAZ, CAS and CA, pseudo-ductile character was prominent at 1000 °C showing fibre pull-out of their fracture surfaces. The composites, CAZ, CAS and CA show the maximum values of flexural strength at 1000 °C; the presence of γ-$Al_2O_3$ in those samples enhanced the flexural strength values.

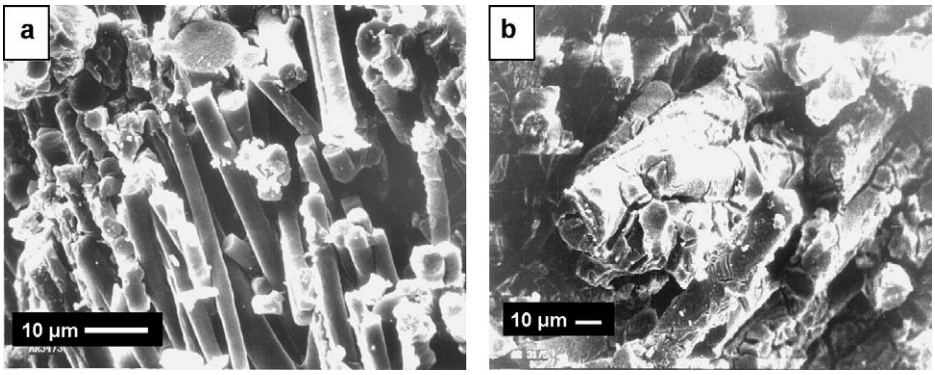


Fig. 7. SEM fractographs of CZY sintered at (a) 1000 °C and (b) 1400 °C after the three-point bending test.

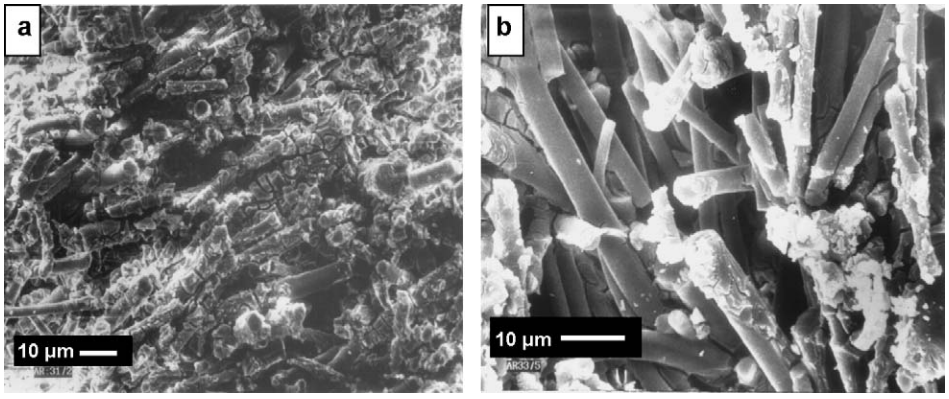


Fig. 8. SEM fractographs of (a) CAZ and (b) CA sintered at 1000 °C each after the three-point bending test.

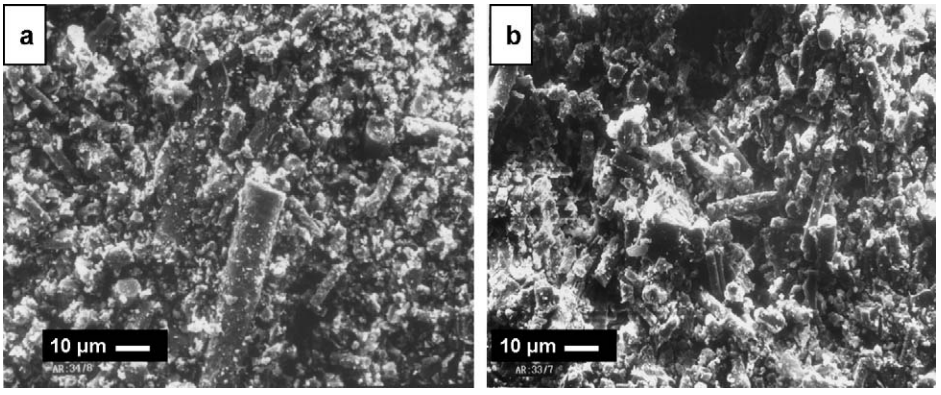


Fig. 9. SEM fractographs of (a) CAS and (b) CA sintered at 1400 °C each after the three-point bending test.

## 4. Conclusions

Sol–gel vacuum infiltration route was followed for the fabrication of near-net-shape CMCs using high alumina fibre preform and various sols of single and bicomponent oxide systems as the infiltrates. The sintering temperature affected the crystallization behaviours of the matrix materials, fibre preforms and composites as well. The flexural strength of the composites was dependent on their state of crystallization. Crystalline phases of the CMCs influenced the fibre–matrix interface optimizing the fibre pull out and pseudo-ductility of the composites. Therefore, the crystallization behaviours of the composites proved to be a key factor in optimizing the characteristics of the CMCs.

## Acknowledgements

The authors thank Dr. H.S. Maiti, Director, Central Glass & Ceramic Research Institute (CG & CRI), Kolkata for his constant encouragement and kind permission to publish this paper. They acknowledge the sincere helps rendered by the colleagues of X-ray Diffraction, SEM & ESCA and Composite Sections of CG & CRI in materials characterization.

## References


[1] R.S. Russel-Floyd, B. Harris, R.G. Cooke, J. Laurie, F.W. Hammett, R.W. Jones, T. Wang, Application of sol–gel processing techniques for the manufacture of fibre-reinforced ceramics, J. Am. Ceram. Soc. 76 (10) (1993) 2635–2643.

[2] K.K. Chawla, Ceramic Matrix Composites, Chapman and Hall, UK, 1993

[3] H.-K. Liu, W.-S. Kuo, B.-H. Lin, Pressure infiltration of sol–gel processed short fibre ceramic matrix composites, J. Mater. Sci. 33 (8) (1998) 2095–2101.

[4] B. Saruhan, M. Bartsch, M. Schmucker, H. Schneider, K. Nubian, G. Wahl, Correlation of high-temperature properties and interphase characteristics in oxide/oxide fibre-reinforced composites, Intl. J. Mater. Prod. Technol. 16 (1–3) (2001) 259–268.

[5] W.B. Hillig, Melt infiltration approach to ceramic matrix composites, J. Am. Ceram. Soc. 71 (2) (1988) c-96c–99.

[6] Y. Zhang, Y. Xu, J. Lou, L. Zhang, L. Cheng, J. Lou, Z. Chen, Braking behaviour of C/SiC composites prepared by chemical vapor infiltration, Intl. J. Appl. Ceram. Technol. 2 (2) (2005) 114–121.

[7] S. Dong, Y. Katoh, A. Kohyama, Processing optimization and mechanical evaluation of hot pressed 2D Tyranno-SA/SiC composites, J. Eur. Ceram. Soc. 23 (2003) 1223–1231.

[8] T. Radsick, B. Saruhan, H. Schneider, Damage tolerant oxide/oxide fiber laminate composites, J. Eur. Ceram. Soc. 20 (2000) 545–550.

[9] S.M. Sim, R.J. Kerans, Slurry infiltration of 3-D woven composites, Ceram. Eng. Sci. Proc. 13 (9–10) (1992) 632–641.

[10] A. Dey, M. Chatterjee, M.K. Naskar, S. Dalui, K. Basu, A novel technique for fabrication of near-net-shape CMCs, Bull. Mater. Sci. 25 (6) (2002) 493–495.

[11] A. Dey, M. Chatterjee, M.K. Naskar, K. Basu, Near-net-shape fibre reinforced ceramic matrix composites by the sol infiltration technique, Mater. Lett. 57 (2003) 2919–2926.

[12] K. Rundgren, P. Elfving, H. Tabata, S. Kanzaki, R. Pompe, Microstructures and mechanical properties of mullite–zirconia composites made from inorganic sols and salts, in: S. Somiya, R.F. Davis, J.A. Pask (Eds.), Ceramic Transactions, vol. 6: Mullite and Mullite Matrix Composites, Am. Ceram. Soc., Westerville, Ohio, 1990, pp. 553–566.

[13] J. Wu, F.R. Jones, P.F. James, Mullite matrix continuous fibre reinforced composites by sol–gel processing, in: J.P. Sing, N.P. Bansal (Eds.), Ceramic Transactions, vol. 46: Advances in Ceramic-Matrix Composites II, The Am. Ceram. Soc., Westerville, Ohio, 1994, pp. 177–187.

[14] M.B. Ruggles-Wrenn, P. Koutsoukos, S.S. Baek, Effects of environment on creep behaviour of two oxide/oxide ceramic-matrix composites at 1200 °C, J. Mater. Sci. 43 (2008) 6734–6746.

[15] J.R. Strife, J.J. Brennan, K.M. Prewo, Status of continuous fibre-reinforced ceramic matrix composite processing technology, Ceram. Eng. Sci. Process. 11 (7–8) (1990) 871–919.

[16] Wang-Zhi, S. Guopu, S. Xiang, H. Xianqin, Mullite fibre reinforced alumina ceramic matrix composites, Eng. Mater. 368–372 (2008) 710–712.

[17] M.K. Naskar, M. Chatterjee, A. Dey, K. Basu, Effects of processing parameters on the fabrication of near-net-shape fibre reinforced oxide ceramic matrix composites via sol–gel route, Ceram. Intl. 30 (2004) 257–265.

[18] C. Rastetter, W.R. Symes, Alumina fibre- a polycrystalline refractory fibre for use up to 1600 °C, Interceramics 31 (3) (1982) 215–220.

[19] J.L. Mcardle, G.L. Messing, Transformation and microstructure control in boehmite- derived alumina by ferric oxide seeding, Adv. Ceram. Mater. 3 (4) (1988) 387–392.